

Your thesaurus codes are:  
08(02.13.2,02.20.1,06.01.2,06.18.2,08.12.1)

# The Maunder minimum as due to magnetic $\Lambda$ -quenching

M. Küker, R. Arlt, and G. Rüdiger

Astrophysikalisches Institut Potsdam, An der Sternwarte 16, D-14482 Potsdam, Germany

Received date; accepted date

**Abstract.** A 2D mean-field MHD code for spheres is used to check the nonlinear interplay between dynamo-induced magnetic fields and the differential rotation in convection zones. The magnetic back-reaction is threefold: Lorentz force,  $\alpha$ -quenching and  $\Lambda$ -quenching. If only the Malkus-Proctor feedback is used then the dynamo shows an interesting nonperiodic behavior which, however, disappears for alpha-quenching included (cf. Fig. 2). If also a strong  $\Lambda$ -quenching is allowed to modify the differential rotation then the dynamo starts its exotic performance again with periodic periods and fluctuating magnetic parities. The Elsasser number has been put to unity whereas the magnetic Prandtl number must be smaller than unity. For too small Prandtl number (e.g. for  $P_m = 0.01$ ), however, the grand minima become very seldom events.

**Key words:** *magnetohydrodynamics* (MHD) – Turbulence – Sun: activity – Sun: rotation – Stars: late-type

## 1. Introduction

The observation of sunspot numbers is the most obvious representation of solar activity. A periodicity of 11 years has been observed for several centuries, but this oscillation is far from sinusoidal. Cycle period as well as amplitude vary considerably around their averages. For example, the quality of the cycle,  $\omega_{\text{cyc}}/\Delta\omega_{\text{cyc}}$ , is as low as 5. Sunspots were even almost entirely absent during the Maunder minimum between 1666 and 1715 (Spörer 1889). Similar lulls of activity, which we will henceforth call grand minima, were detected after the Maunder minimum and before it back to early medieval times. Much longer time series than sunspot counts derive from measurements of  $^{14}\text{C}$  abundances in sediments and long-lived trees. Schwarz (1994) found in agreement with Vos et al. (1997) a secular periodicity of 80–90 yr as well as a long-duration period of about 210 yr. The measurements of atmospheric  $^{14}\text{C}$  abundances by Hood & Jirikowic (1990) suggested a periodicity of 2400 yr which is also associated with a long-term variation of solar activity. A multitude of frequencies in the activity

of the Sun may even indicate a chaotic behavior as discussed by Rozelot (1995).

The activity cycle of the Sun is not exceptional: The observations of chromospheric Ca-emission of solar-type stars yielded activity periods between 3 and 20 yrs (Noyes et al. 1984, Baliunas & Vaughan 1985, Saar & Baliunas 1993a,b). A few stars among them without significant activity suggest that even the existence of grand minima is a typical property of cool main-sequence stars like the Sun. With ROSAT X-ray data Hempelmann et al. (1996) find that up to 70% of the constant stars exhibit only a low level of coronal X-ray emission. E.g. HD 142373 with its X-luminosity of only  $\log F_X = 3.8$  is a typical candidate. We conclude that during a grand minimum not only the magnetic belts (producing the dark spots) are weak but even the total magnetic energy does so.

The wavelet analysis of sunspot data by Frick et al. (1997) indicates a decrease of the short-term cycle period at the end of, or even through (if periods are detectable) a grand minimum. The distribution of latitudinal positions of the few Maunder minimum sunspots was highly asymmetric (Ribes & Nesme-Ribes 1993, Nesme-Ribes et al. 1994). Short-term deviations from the north-south symmetry in regular solar activity are readily observable (Verma 1993), yet a 30-year period of asymmetry in sunspot positions as seen during the Maunder minimum (cf. Spörer 1889) remains a unique property of grand minima and should be associated with a parity change of the driving internal magnetic fields.

After Wittmann (1978) and very recently Beer et al. (1998) there is empirical evidence for an overall existence of the solar cycle even throughout the Maunder minimum but, of course, with a drastic reduction of the amplitude.

## 2. Mean-field electrodynamics

There are so far two concepts for dynamo-induced grand minima of cyclic magnetic activity. The first one bases on the idea that due to the stochastic character of the turbulence its statistical properties and hence the  $\alpha$ -effect and all related phenomena vary with time (Choudhuri 1992, Hoyng 1993, Hoyng et al. 1994, Ossendrijver 1996, Schmitt et al. 1996, Otmianowska-Mazur et al. 1997). The second one works with the inclusion

of the magnetic feedback to the internal solar rotation (Weiss et al. 1984, Jennings & Weiss 1991). Kitchatinov et al. (1994) and Tobias (1996, 1997) even introduced the conservation law of angular momentum in the turbulent convection zone including magnetic feedback in order to produce grand minima of the dynamo cycle. In the present paper we for the first time present a 2D spherical mean-field theory on the basis of a solar overshoot dynamo model (Rüdiger & Brandenburg 1995) together with a theory of differential rotation based on the  $\Lambda$ -effect concept (Küker et al. 1993, Kitchatinov & Rüdiger 1993).

We assume axial symmetry of the hydromagnetic state for the star and ignore meridional flows. Then the mean velocity and magnetic fields in spherical coordinates  $(r, \theta, \phi)$  are

$$U = (0, 0, r \sin \theta \Omega(r, \theta, t)), \quad (1)$$

$$B = \left( \frac{1}{r^2 \sin \theta} \frac{\partial A(r, \theta, t)}{\partial \theta}, -\frac{1}{r \sin \theta} \frac{\partial A(r, \theta, t)}{\partial r}, B(r, \theta, t) \right), \quad (2)$$

where  $A$  is the poloidal-field potential,  $B$  is the toroidal field and  $\Omega$  is the angular velocity.

The field equations for the convection zone include the effects of diffusion,  $\alpha$ -effect, toroidal field production by differential rotation and the Lorentz force. They read

$$\begin{aligned} \rho r \sin \theta \frac{\partial \Omega}{\partial t} = & -\frac{1}{r^3} \frac{\partial}{\partial r} (r^3 \rho Q_{r\phi}) - \frac{1}{r \sin^2 \theta} \frac{\partial}{\partial \theta} (\sin^2 \theta \rho Q_{\theta\phi}) + \\ & + \frac{1}{\mu_0 r^2 \sin \theta} \left( \frac{1}{r} \frac{\partial A}{\partial \theta} \frac{\partial (Br)}{\partial r} - \frac{1}{\sin \theta} \frac{\partial A}{\partial r} \frac{\partial (B \sin \theta)}{\partial \theta} \right), \quad (3) \end{aligned}$$

$$\begin{aligned} \frac{\partial B}{\partial t} = & \frac{1}{r} \frac{\partial}{\partial r} \left( \eta_{\Gamma} \frac{\partial (Br)}{\partial r} \right) + \frac{\eta_{\Gamma}}{r^2} \frac{\partial}{\partial \theta} \left( \frac{1}{\sin \theta} \frac{\partial (B \sin \theta)}{\partial \theta} \right) + \\ & + \frac{1}{r} \frac{\partial \Omega}{\partial r} \frac{\partial A}{\partial \theta} + \frac{1}{r} \frac{\partial \Omega}{\partial \theta} \frac{\partial A}{\partial r} - \frac{1}{r \sin \theta} \frac{\partial}{\partial r} \left( \alpha \frac{\partial A}{\partial r} \right) - \\ & - \frac{1}{r^3} \frac{\partial}{\partial \theta} \left( \frac{\alpha}{\sin \theta} \frac{\partial A}{\partial \theta} \right), \quad (4) \end{aligned}$$

$$\frac{\partial A}{\partial t} = \eta_{\Gamma} \frac{\partial^2 A}{\partial r^2} + \eta_{\Gamma} \frac{\sin \theta}{r^2} \frac{\partial}{\partial \theta} \left( \frac{1}{\sin \theta} \frac{\partial A}{\partial \theta} \right) + \alpha r \sin \theta B \quad (5)$$

(Rüdiger 1989), where  $\rho$  denotes the density while  $\nu_{\Gamma}$  and  $\eta_{\Gamma}$  are the viscosity and magnetic diffusivity, correspondingly. As usual,  $Q_{ij}$  is the one-point correlation tensor of the convection turbulence,  $Q_{ij} = \langle u'_i u'_j \rangle$ .

The domain of the computations covers the outer parts of the Sun down to a fractional solar radius,  $x = r/R$ , of 0.5. The convection zone extends from  $x = 0.7$  to  $x = 1$ . The  $\alpha$ -effect works only in the lower part from  $x = 0.7$  to  $x = 0.8$  while turbulent diffusion of the magnetic field, turbulent viscosity, and the  $\Lambda$ -effect are present in the whole convection zone. Below  $x = 0.7$ , both the magnetic diffusivity and the viscosity are

two orders of magnitude smaller than in the convection zone. The boundary conditions are specified as

$$Q_{r\phi} = \frac{\partial A}{\partial r} = B = 0 \quad \text{at } r = R, \quad (6)$$

and

$$Q_{r\phi} = A = B = 0 \quad (7)$$

at the inner boundary. The fluxes of angular momentum are

$$\begin{aligned} Q_{r\phi} &= \nu_{\Gamma} \sin \theta \left( -r \frac{\partial \Omega}{\partial r} + V^{(0)} \Omega \right), \\ Q_{\theta\phi} &= -\nu_{\Gamma} \sin \theta \frac{\partial \Omega}{\partial \theta}. \quad (8) \end{aligned}$$

$V^{(0)}$  determines the rotation law without magnetic field. Our equations are renormalized with

$$r = R \tilde{r}, \quad t = \frac{R^2}{\eta_{\Gamma}} \tilde{t}, \quad \Omega = \Omega_0 \tilde{\Omega} \quad (9)$$

as well as with

$$A = R^2 B_{\text{eq}} \tilde{A}, \quad B = B_{\text{eq}} \tilde{B}. \quad (10)$$

$B_{\text{eq}}$  is the turbulence-equipartition field defined below. After insertion of the relations into (3)–(5) we arrive at the system of dimensionless equations

$$\begin{aligned} \frac{\partial \Omega}{\partial t} = & \frac{\text{Pm}}{r^4} \frac{\partial}{\partial r} \left( r^3 \left( r \frac{\partial \Omega}{\partial r} - V^{(0)} \Omega \right) \right) + \\ & + \frac{\text{Pm}}{r^2 \sin^3 \theta} \frac{\partial}{\partial \theta} \left( \sin^3 \theta \frac{\partial \Omega}{\partial \theta} \right) + \\ & + \frac{\text{E}}{r^2 \sin \theta} \left( \frac{1}{r} \frac{\partial A}{\partial \theta} \frac{\partial (rB)}{\partial r} - \frac{1}{\sin \theta} \frac{\partial A}{\partial r} \frac{\partial}{\partial \theta} (\sin \theta B) \right), \quad (11) \end{aligned}$$

$$\frac{\partial A}{\partial t} = \frac{\partial^2 A}{\partial r^2} + \frac{\sin \theta}{r^2} \frac{\partial}{\partial \theta} \left( \frac{1}{\sin \theta} \frac{\partial A}{\partial \theta} \right) + r \sin \theta C_{\alpha} \alpha B, \quad (12)$$

$$\begin{aligned} \frac{\partial B}{\partial t} = & \frac{1}{r} \frac{\partial^2}{\partial r^2} (rB) + \frac{1}{r^2} \frac{\partial}{\partial \theta} \left( \frac{1}{\sin \theta} \frac{\partial}{\partial \theta} (\sin \theta B) \right) + \\ & + \frac{C_{\Omega}}{r} \frac{\partial \Omega}{\partial r} \frac{\partial A}{\partial \theta} + \frac{C_{\Omega}}{r} \frac{\partial \Omega}{\partial \theta} \frac{\partial A}{\partial r} - \\ & - \frac{C_{\alpha}}{r \sin \theta} \frac{\partial}{\partial r} \left( \alpha \frac{\partial A}{\partial r} \right) - \frac{C_{\alpha}}{r^3} \frac{\partial}{\partial \theta} \left( \frac{\alpha}{\sin \theta} \frac{\partial A}{\partial \theta} \right). \quad (13) \end{aligned}$$

The model is defined by five dimensionless numbers, namely the magnetic Reynolds numbers of differential rotation and  $\alpha$ -effect,

$$C_{\Omega} = \frac{\Omega_0 R^2}{\eta_{\Gamma}}, \quad C_{\alpha} = \frac{\alpha_0 R}{\eta_{\Gamma}}, \quad (14)$$

the magnetic Prandtl number

$$\text{Pm} = \frac{\nu_{\Gamma}}{\eta_{\Gamma}}, \quad (15)$$

the Elsasser number

$$E = \frac{B_{\text{eq}}^2}{\mu_0 \rho \eta_T \Omega_0}, \quad (16)$$

and the strength of the  $\Lambda$ -effect,  $V^{(0)}$ . In (14),  $\alpha_0$  is the dynamo-alpha amplitude. The equipartition value of the magnetic field is given by

$$B_{\text{eq}} = \sqrt{\mu_0 \rho \langle u'^2 \rangle}, \quad (17)$$

where  $\langle u'^2 \rangle$  is the mean intensity of the turbulent velocity field. The eddy diffusivity is

$$\eta_T = c_\eta \langle u'^2 \rangle \tau_{\text{corr}}, \quad (18)$$

so that

$$E = \frac{2}{c_\eta \Omega^*}. \quad (19)$$

The Coriolis number  $\Omega^* = 2\tau_{\text{corr}}\Omega_0$  gives the normalized basic rotation. In the  $\alpha$ -effect,

$$\alpha = \alpha_0 \cos \theta \sin^2 \theta, \quad (20)$$

the factor  $\sin^2 \theta$  has been introduced to restrict magnetic activity to low latitudes and  $\alpha_0 \simeq l_{\text{corr}} \Omega_0$ , so that

$$|C_\alpha| \simeq \frac{\Omega_0 R}{c_\eta u'}. \quad (21)$$

Similarly we find

$$\frac{C_\Omega}{|C_\alpha|} \simeq \frac{R}{l_{\text{corr}}}, \quad (22)$$

hence in general the  $C_\Omega$  exceeds  $C_\alpha$  (' $\alpha\Omega$  dynamo'). Our dynamo works with  $C_\alpha = -10$  and  $C_\Omega = 10^5$ .  $V^{(0)}$  is positive in order to produce the required super-rotation, its amplitude is 0.37.

### 3. Results and discussion

Figures 1–4 demonstrate the action of different effects. Each graph shows the variation of the magnetic field at a certain point ( $r = 0.75$  which is the center of the dynamo zone,  $\theta = +30^\circ$ ), the total magnetic energy, the variation of the cycle period, and the parity

$$P = \frac{E_S - E_A}{E_S + E_A}, \quad (23)$$

derived from the decomposition of the magnetic energy into symmetric and antisymmetric components (Brandenburg et al. 1989, 1990). All times and periods are given in units of a diffusion time  $R^2/\eta_T$ . Field strengths are measured in units of  $B_{\text{eq}}$  (17).

Fig. 1 shows the results of a model with the Malkus-Proctor effect as the only feedback on rotation and may be compared with the results in Tobias (1996), although a number of assumptions are different between Tobias' Cartesian approach and our spherical model. Fig. 1 shows a quasi-periodic behavior with

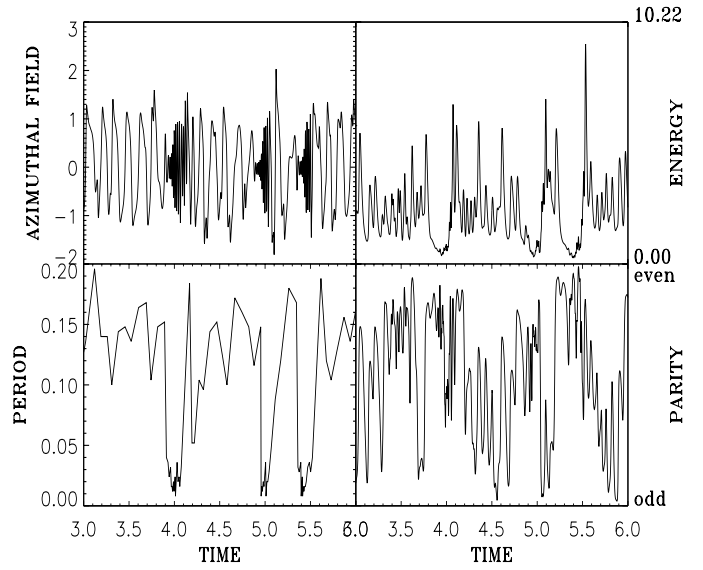


**Fig. 1.** The time dependence of the dynamo basics for the magnetic Malkus-Proctor feedback only (i.e. without both  $\alpha$ -quenching and  $\Lambda$ -quenching,  $\text{Pm} = 0.1$ ,  $E = 1$ ). TOP: Toroidal magnetic field (left) and magnetic energy (right). BOTTOM: Cycle time (left) and magnetic parity (right)

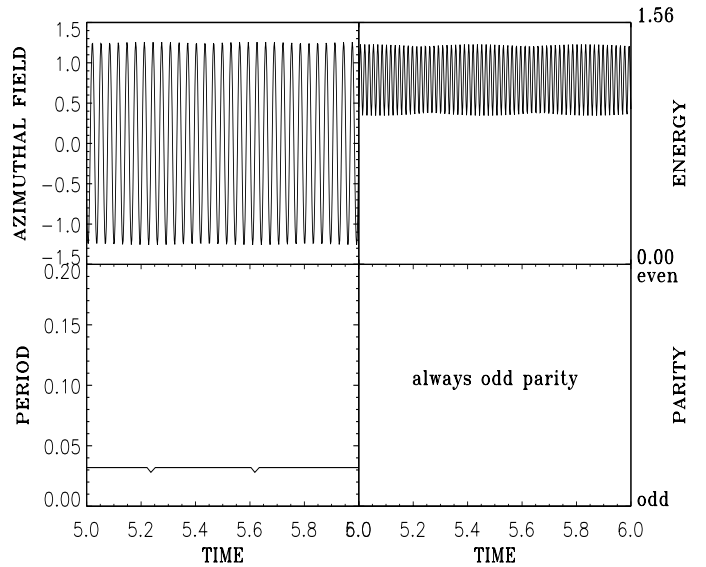


**Fig. 2.** The same as in Fig. 1 but with  $\alpha$ -quenching and without  $\Lambda$ -quenching ( $\lambda = 0$ ). TOP: Toroidal magnetic field (left) and magnetic energy (right). BOTTOM: Cycle time (left) and magnetic parity (right)

interruptions in activity like grand minima. This model, however, neglects the feedback of strong magnetic fields on the  $\alpha$ -effect and the differential rotation.

The same model but with local  $\alpha$ -quenching

$$\alpha \propto \frac{1}{1 + (B_{\text{tot}}/B_{\text{eq}})^2} \quad (24)$$

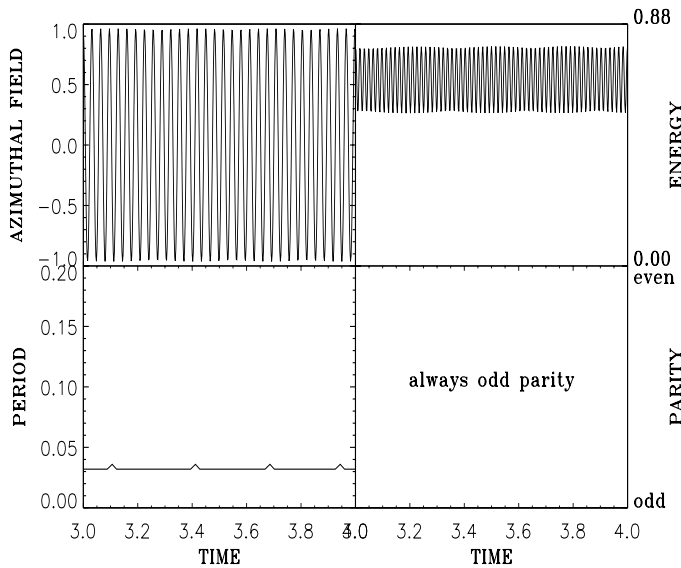


**Fig. 3.** The same as in Fig. 2 but with  $\Lambda$ -quenching ( $\lambda = 1$ ). TOP: Toroidal magnetic field (left) and magnetic energy (right). BOTTOM: Cycle time (left) and magnetic parity (right)

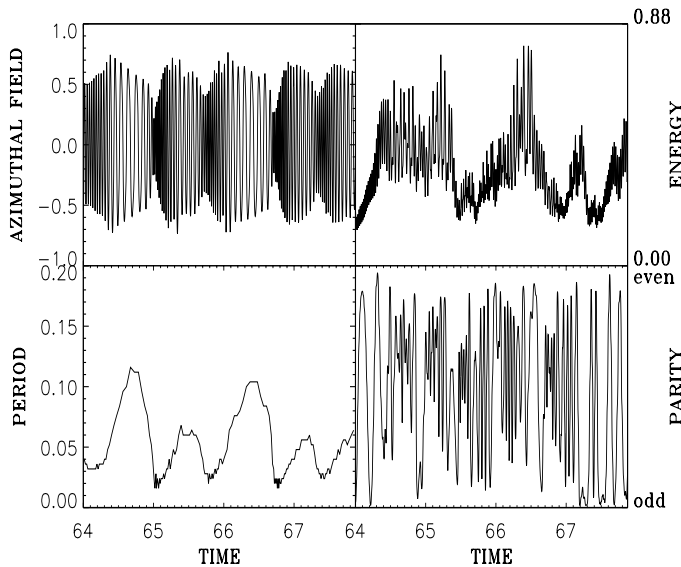


**Fig. 4.** The same as in Fig. 3 but for strong  $\Lambda$ -quenching ( $\lambda = 25$ ). TOP: Toroidal magnetic field (left) and magnetic energy (right). BOTTOM: Cycle time (left) and magnetic parity (right)

is used for Fig. 2, where  $B_{\text{tot}}$  is the absolute value of the magnetic field. A one-period solution appears, since magnetic fields are suppressed before the nonlinearity due to the Malkus-Proctor feedback disturbs the oscillatory behavior of the  $\alpha^2\Omega$ -dynamo. The period of a mere  $\alpha^2\Omega$ -dynamo with  $\alpha$ -quenching is 0.023 in units of Figs. 1–4.

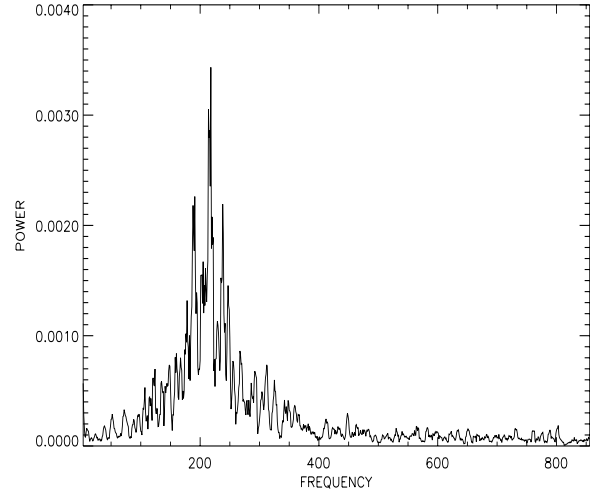


**Fig. 5.** Power spectrum of the magnetic-field amplitude variations for the ‘Malkus-Proctor’ model of Fig. 1. The frequency is given in arbitrary units

Similarly to the suppression of dynamo action, a quenching of the  $\Lambda$ -effect causing the differential rotation is applied by

$$V^{(0)} \propto \frac{1}{1 + \lambda(B_{\text{tot}}/B_{\text{eq}})^2}. \quad (25)$$

Just a decrease in maximum field strength and total magnetic energy is shown in Fig. 3 for  $\lambda = 1$ ; the periodic behavior remains the same, i.e. the effect of the  $\Lambda$ -quenching is too small to alter the differential rotation significantly. However, *an increase of  $\lambda$  leads to grand minima* – an example for  $\lambda = 25$  is given in Fig. 4. In agreement with observational sunspot data (cf. Frick et al. 1997), a minimum of the cycle period occurs *shortly after* the grand minimum. The solar cycle period varies between 9 and 13 yrs, but it is unknown for the time of the Maunder minimum. The amplitude of the periodicity fluctuations is much higher in the Malkus-Proctor model. Although these variations are weaker in the full model shown in Fig. 4, they are still higher than those observed. In all our cases the magnetic Prandtl number is  $\text{Pm} = 0.1$ . For  $\text{Pm} = 1.0$ , however, grand minima *do not appear* in models as in Fig. 1 and 4.

The parity for the non-periodic results in Figs. 1 and 4 shows strong variations between purely symmetric and anti-symmetric solutions. It should be noted that the dynamo zone is filled with several (usually 5–6) magnetic-field belts migrating towards the equator. Slight shifts of this belt-structure against the equator result in strong variations in the parity. Averaged over time, dipolar and quadrupolar components of the fields have roughly the same strength; all periodic solutions (e.g. Figs. 2 and 3) have purely dipolar structure.

The periodicities of the magnetic field can be analyzed with spectra of very long time series. Figs. 5 and 6 show the spectra of the Malkus-Proctor model and the strong- $\Lambda$ -quenching model, resp. The long-term variations of the field will be represented by a set of close frequencies whose difference is the fre-

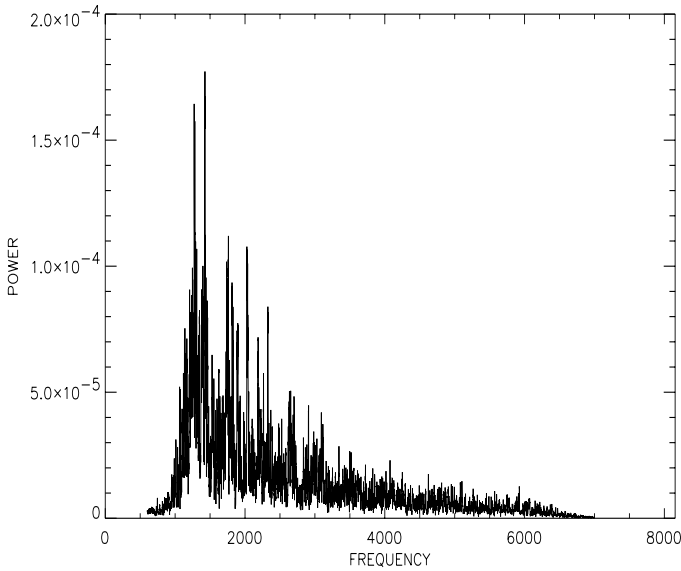


**Fig. 6.** The same as in Fig. 5 but for the model with strong  $\Lambda$ -quenching given in Fig. 4

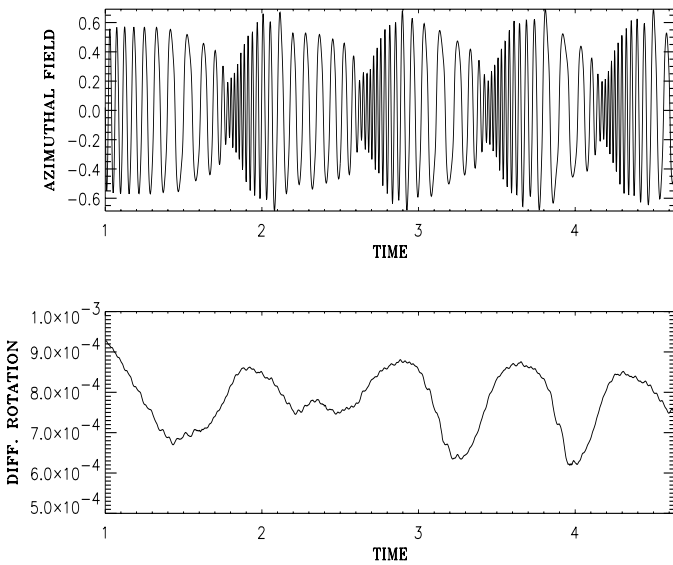


**Fig. 7.** Correlation between magnetic field oscillations and variations of the differential rotation measure  $(\partial\Omega/\partial r)^2$ , averaged over the latitude  $\theta$ .

quency of the grand minima. The Malkus-Proctor model shows a number of lines close to the main cycle frequency. The difference between the highest peaks can be interpreted as the occurrence rate of grand minima. However, the shape of the spectrum indicates that the magnetic-field appears rather irregularly. The spectrum of the model with all feedback terms and strong  $\Lambda$ -quenching is given in Fig. 6 and shows a similar behavior with highest amplitudes near the main cycle frequency of the magnetic field. The average frequency of the grand minima is represented by the distance of the highest peaks.

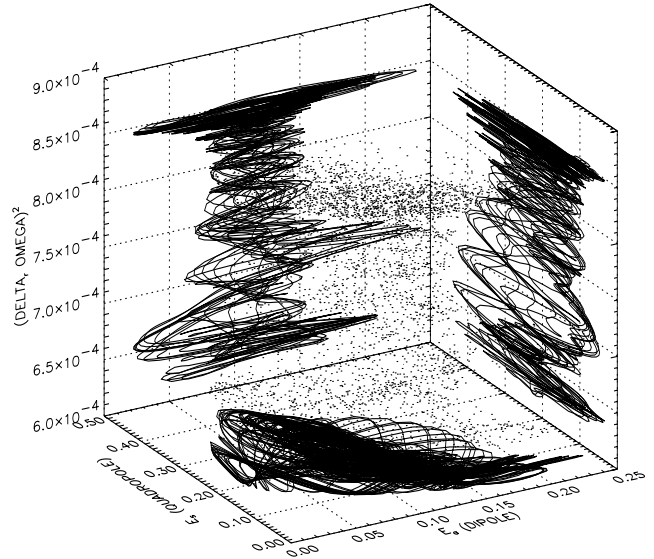


**Fig. 8.** Correlations between magnetic field energies for both parities (dipolar and quadrupolar) and the differential rotation. The radial gradient of the angular velocity is taken at the equator

Fig. 7 shows the variations of the radial difference of the rotation rate averaged over  $\theta$ ,  $\langle(\partial\Omega/\partial r)^2\rangle$ , versus time, compared to the magnetic field taken from Fig. 4. A minimum in differential rotation is accompanied by a decay of magnetic fields and followed by a grand minimum. The differential rotation is being restored during the grand minimum since the suppressing effect of magnetic  $\Lambda$ -quenching is reduced.

The correlation between the dipolar component  $E_A$  of the magnetic field, the quadrupolar component  $E_S$  and the angular velocity gradient is shown in Fig. 8. The differential rotation is again measured in terms of  $(\partial\Omega/\partial r)^2$ , averaged over the latitude  $\theta$  as in Fig. 7. The dots in the interior of the diagram represent the actual time series; projections of the trajectory are given at the sides. The phase graph is similar to those given in Knobloch et al. (1998).

The trajectory resides at strong differential rotation during normal cyclic activity. The magnetic field oscillates in a wide range of energies. The trajectory moves down as the fields start to suppress differential rotation, with oscillation amplitudes diminishing. The actual grand minimum is expressed by a loop at very low dipolar energies; the quadrupolar component, however, keeps present throughout the minimum. Like in Fig. 7, the differential-rotation measure is already growing at that time. At first glance, the phase graph may be associated with Type 1 modulation as classified in Knobloch et al. (1998).

#### 4. Summary

We can summarize the results as follows: When only considering large-scale Lorentz forces on the differential rotation, one gets irregular grand minima with strong variations in cycle period (with a factor of 20). If the suppression of dynamo action ( $\alpha$ -quenching) is included, the dynamo returns to oscilla-

tions with one frequency. If a strong feedback of small-scale flows on the generation of Reynolds stress ( $\Lambda$ -quenching) is included, grand minima occur at a reasonable rate between 10 and 20 cycle times. The cycle period varies by a factor of 6–8. Northern hemisphere and southern hemisphere slightly differ in their temporal behavior. This is a general characteristics of mixed-modes dynamo explanations of grand minima.

In any case, Prandtl numbers smaller than unity are required for the existence of grand minima. However, the magnetic Prandtl number directs the Intermittency of the activity cycle. For small values of  $Pm$  the occurrence of grand minima again becomes more and more exceptional (Fig. 9).

*Acknowledgements.* M.K. and R.A. thank for the support by the Deutsche Forschungsgemeinschaft. The authors are grateful to A. Brandenburg for a critical reading of the manuscript.

## References

- Baliunas S. L., Vaughan A. H., 1985, *ARA&A* 23, 379  
 Beer J., Tobias S. M., Weiss N. O., 1998, *Solar Phys.* (to appear)  
 Brandenburg A., Krause F., Meinel R., Moss D., Tuominen I., 1989, *A&A* 213, 411  
 Brandenburg A., Meinel R., Moss D., Tuominen I., 1990, Variation of even and odd parity in the solar dynamo. In: Stenflo J.O. (ed.) *Solar Photosphere: Structure, Convection, and Magnetic Fields*. Verlag, Ort, p. 379  
 Choudhuri A. R., 1992, *A&A* 253, 277  
 Frick P., Galyagin D., Hoyt D. V., Nesme-Ribes E., Schatten K. H., Sokoloff D., Zakharov V., 1997, *A&A* 328, 670  
 Hempelmann A., Schmitt J., Stepień K., 1996, *A&A* 305, 284  
 Hood L. L., Jirikovic, J. L., 1990, A probable approx. 2400 year solar quasi-cycle in atmospheric  $\delta C-14$ . In: NASA, Goddard Space Flight Center, *Climate Impact of Solar Variability*. Arizona Univ., Tucson, p. 98  
 Hoyng P., 1993, *A&A* 272, 321  
 Hoyng P., Schmitt D., Teuben L. J. W., 1994, *A&A* 289, 265  
 Jennings R. L., Weiss N. O., 1991, *MNRAS* 252, 249  
 Kitchatinov L. L., Rüdiger G., 1993, *A&A* 276, 96  
 Kitchatinov L. L., Rüdiger G., Küker M., 1994, *A&A* 292, 125 (Paper I)  
 Knobloch E., Tobias S.M., Weiss N.O., 1998, *MNRAS* 297, 1123  
 Küker M., Rüdiger G., Kitchatinov L. L., 1993, *A&A* 279, 1  
 Malkus W. V. R., Proctor M. R. E., 1975, *J. Fluid Mech.* 67, 417  
 Nesme-Ribes E., Sokoloff D., Ribes J. C., Kremlivsky M., 1994, The Maunder minimum and the solar dynamo. In: Nesme-Ribes E. (ed.) *NATO ASI Series, The Solar Engine and Its Influence on Terrestrial Atmosphere and Climate*. Springer-Verlag, Berlin, p. 71  
 Noyes R. W., Weiss N. O., Vaughan A. H., 1984, *ApJ* 287, 769  
 Ossendrijver M., 1996, *A&A* 313, 959  
 Otmianowska-Mazur K., Rüdiger G., Elstner D., Arlt R., 1997, *GAFD* 86, 229  
 Ribes J. C., Nesme-Ribes E., 1993, *A&A* 276, 549  
 Rozelot J. P., 1995, *A&A* 297, L45  
 Rüdiger G., 1989, *Differential rotation and stellar convection: Sun and solar-type stars*, Gordon and Breach Science Publishers, New York  
 Rüdiger G., Brandenburg A., 1995, *A&A* 296, 557  
 Baliunas S. L., Vaughan A. H., 1985, *ARA&A* 23, 379  
 Beer J., Tobias S. M., Weiss N. O., 1998, *Solar Phys.* (to appear)  
 Brandenburg A., Krause F., Meinel R., Moss D., Tuominen I., 1989, *A&A* 213, 411  
 Brandenburg A., Meinel R., Moss D., Tuominen I., 1990, Variation of even and odd parity in the solar dynamo. In: Stenflo J.O. (ed.) *Solar Photosphere: Structure, Convection, and Magnetic Fields*. Verlag, Ort, p. 379  
 Choudhuri A. R., 1992, *A&A* 253, 277  
 Frick P., Galyagin D., Hoyt D. V., Nesme-Ribes E., Schatten K. H., Sokoloff D., Zakharov V., 1997, *A&A* 328, 670  
 Hempelmann A., Schmitt J., Stepień K., 1996, *A&A* 305, 284  
 Hood L. L., Jirikovic, J. L., 1990, A probable approx. 2400 year solar quasi-cycle in atmospheric  $\delta C-14$ . In: NASA, Goddard Space Flight Center, *Climate Impact of Solar Variability*. Arizona Univ., Tucson, p. 98  
 Hoyng P., 1993, *A&A* 272, 321  
 Hoyng P., Schmitt D., Teuben L. J. W., 1994, *A&A* 289, 265  
 Jennings R. L., Weiss N. O., 1991, *MNRAS* 252, 249  
 Kitchatinov L. L., Rüdiger G., 1993, *A&A* 276, 96  
 Kitchatinov L. L., Rüdiger G., Küker M., 1994, *A&A* 292, 125 (Paper I)  
 Knobloch E., Tobias S.M., Weiss N.O., 1998, *MNRAS* 297, 1123  
 Küker M., Rüdiger G., Kitchatinov L. L., 1993, *A&A* 279, 1  
 Malkus W. V. R., Proctor M. R. E., 1975, *J. Fluid Mech.* 67, 417  
 Nesme-Ribes E., Sokoloff D., Ribes J. C., Kremlivsky M., 1994, The Maunder minimum and the solar dynamo. In: Nesme-Ribes E. (ed.) *NATO ASI Series, The Solar Engine and Its Influence on Terrestrial Atmosphere and Climate*. Springer-Verlag, Berlin, p. 71  
 Noyes R. W., Weiss N. O., Vaughan A. H., 1984, *ApJ* 287, 769  
 Ossendrijver M., 1996, *A&A* 313, 959  
 Otmianowska-Mazur K., Rüdiger G., Elstner D., Arlt R., 1997, *GAFD* 86, 229  
 Ribes J. C., Nesme-Ribes E., 1993, *A&A* 276, 549  
 Rozelot J. P., 1995, *A&A* 297, L45  
 Rüdiger G., 1989, *Differential rotation and stellar convection: Sun and solar-type stars*, Gordon and Breach Science Publishers, New York  
 Rüdiger G., Brandenburg A., 1995, *A&A* 296, 557  
 Saar S. H., Baliunas S. L., 1993a, Recent advances in stellar cycle research. In: Harvey K. L. (ed.) *The Solar Cycle Workshop*. ASP Conf. Series 27, p. 150  
 Saar S. H., Baliunas S. L., 1993b, The magnetic cycle of  $\kappa$  Ceti (G5V). In: Harvey K. L. (ed.) *The Solar Cycle Workshop*. ASP Conf. Series 27, p. 197  
 Schmitt D., Schüssler M., Ferriz-Mas A., 1996, *A&A* 311, L1  
 Schwarz U., 1994, Dissertation, Universität Potsdam  
 Sokoloff D., Nesme-Ribes E., 1994, *A&A* 288, 293  
 Spörer G., 1889, *Verhandl. Kgl. Leopold.-Carol. Deutschen Akad. Naturf.* 53, 283  
 Tobias S. M., 1996, *A&A* 307, L21  
 Tobias S. M., 1997, *A&A* 322, 1007  
 Verma V. K., 1993, *ApJ* 403, 797  
 Vos H., Sanchez A., Zolitschka B., Brauer A., Negendank J.F.W., 1997, *Surv. Geophys.* 18, 163  
 Weiss N. O., Cattaneo F., Jones C. A., 1984, *GAFD* 30, 305  
 Wittmann A., 1978, *A&A* 66, 93

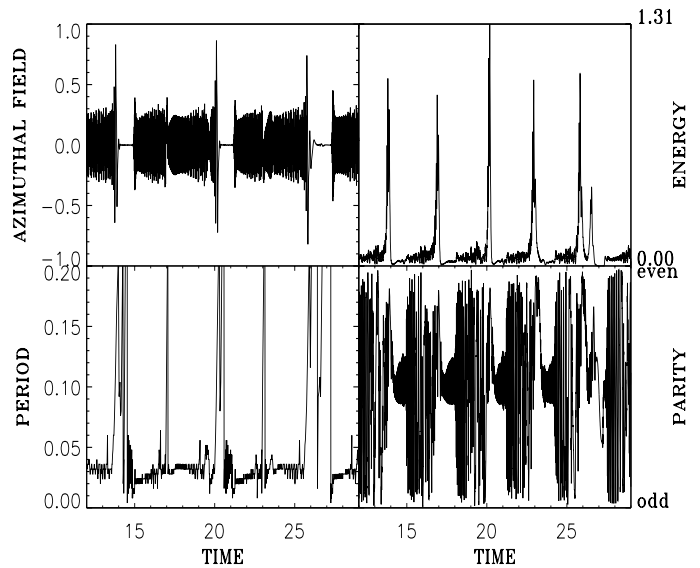


**Fig. 9.** The same as in Fig. 4 but for  $Pm=0.01$ . The grand minima are much more seldom than for  $Pm=0.1$